JBC ARTICLE

Atomic-resolution map of the interactions between an amyloid inhibitor protein and amyloid β (Aβ) peptides in the monomer and protofibril states

Received for publication, April 23, 2017, and in revised form, August 8, 2017 Published, Papers in Press, August 10, 2017, DOI 10.1074/jbc.M117.792853

Moustafa Algamal[‡], Rashik Ahmed[§], Naeimeh Jafari[‡], Bilal Ahsan[§], Joaquin Ortega[§], and Giuseppe Melacini[‡§1]

From the Departments of [‡]Chemistry and Chemical Biology and [§]Biochemistry and Biomedical Sciences, McMaster University, Hamilton, Ontario L8S 4M1, Canada

Edited by Wolfgang Peti

Self-association of amyloid β (Aβ) peptides is a hallmark of Alzheimer's disease and serves as a general prototype for amyloid formation. A key endogenous inhibitor of Aβ self-association is human serum albumin (HSA), which binds ~90% of plasma Aβ. However, the exact molecular mechanism by which HSA binds Aβ monomers and protofibrils is not fully understood. Here, using dark-state exchange saturation transfer NMR and relaxation experiments complemented by morphological characterization, we mapped the HSA-Aβ interactions at atomic resolution by examining the effects of HSA on Aβ monomers and soluble high-molecular weight oligomeric protofibrils. We found that HSA binds both monomeric and protofibrillar Aβ, but the affinity of HSA for Aβ monomers is lower than for Aβ protofibrils (K_d values are submillimolar rather than micromolar) yet physiologically relevant because of the ~0.6–0.7 mM plasma HSA concentration. In both Aβ protofibrils and monomers, HSA targets key Aβ self-recognition sites spanning the β strands found in cross-β protofibril structures, leading to a net switch from direct to tethered contacts between the monomeric Aβ and the protofibril surface. These HSA-Aβ interactions are isoform-specific, because the HSA affinity of Aβ monomers is lower for Aβ(1–42) than for Aβ(1–40). In addition, the HSA-induced perturbations of the monomer/protofibrils pseudo-equilibrium extend to the C-terminal residues in the Aβ(1–42) isoform but not in Aβ(1–40). These results provide an unprecedented view of how albumin interacts with Aβ and illustrate the potential of dark-state exchange saturation transfer NMR in mapping the interactions between amyloid-inhibitory proteins and amyloidogenic peptides.

The exact etiology of Alzheimer's disease is not fully understood, but the amyloid cascade hypothesis rationalizes a critical subset of the molecular phenotypes linked to the pathology of Alzheimer's disease (1). According to the amyloid hypothesis, the aggregation of Aβ[2] peptides in the brain contributes to the neuronal death and brain damage typically observed in Alzheimer's patients. The Aβ peptides are present in both the cerebrospinal fluid (CSF) and in blood plasma, but in the latter the self-association of Aβ into amyloids is inhibited primarily by human serum albumin (HSA), which binds ~90% of plasma Aβ (2, 3). The inhibition of Aβ self-association by HSA has both pathological implications and therapeutic potential (4–7). Low serum albumin concentrations have been reported to be associated with increased cognitive impairment in elderly patients (4), and plasmapheresis with therapeutic albumin is currently being assessed in clinical trials as a potential treatment for mild to moderate Alzheimer's disease (8, 9). The pathological and therapeutic potential of HSA warrants a comprehensive understanding of the molecular mechanism underlying the HSA-Aβ interactions, not only to improve the HSA therapeutic efficiency but also to elucidate basic principles of amyloid inhibition that will facilitate the design of new amyloid inhibitors (10–17).

Although it is known that albumin inhibits amyloid formation by binding Aβ protofibrils with higher affinity than Aβ monomers and interfering with Aβ protofibrils-monomer recognition (11–13, 18–20), several questions remain open about the molecular mechanism through which HSA prevents Aβ aggregation. First, because of the transient and elusive nature of the protofibrils formed under physiological conditions by the two major physiological species of Aβ, *i.e.* 1–40 and 1–42 (21–24), it is currently not fully understood how protofibrils are perturbed by HSA. Addressing this question is critical to explain how HSA modulates Aβ self-association (11–13). Second, it is currently unclear to what extent and how monomeric Aβ peptides bind HSA in plasma. Although the affinity of HSA for Aβ monomers is expected to be weak (25), the HSA concentration in plasma is high (~0.6–0.7 mM), and therefore low-affinity interactions with HSA ($K_d \leq$ mM) are of potential physiological relevance.

To address these questions, we have prepared solutions of Aβ(1–40) and Aβ(1–42) either diluted to a primarily monomeric form or in a dynamic pseudo-equilibrium between monomers and high-molecular weight oligomeric protofibrils, stabi-

This work was supported by Grant RGPIN-2014-04514 from the Natural Sciences and Engineering Research Council of Canada (to G. M.). The authors declare that they have no conflicts of interest with the contents of this article.

[S] This article contains supplemental text, references, and Figs. S1–S12.

[1] To whom correspondence should be addressed: McMaster University, 1280 Main St. W., Hamilton, ON L8S 4M1. Canada. E-mail: melacin@mcmaster.ca.

[2] The abbreviations used are: Aβ, amyloid β; Aβ40$_n$, Aβ40 protofibrils; Aβ42$_n$, Aβ42 protofibrils; Aβ40$_1$, Aβ40 monomers; Aβ42$_1$, Aβ42 monomers; CSF, cerebrospinal fluid; DEST, dark-state exchange saturation transfer; DLS, dynamic light scattering; HSA, human serum albumin; HSQC, heteronuclear single quantum coherence correlation; STD, saturation transfer difference; Θ, one-point DEST.

lized through the use of low temperatures and desalting, as previously described (26). Under these experimental conditions, the interactions between monomeric Aβ(1–40) or Aβ(1–42), denoted here as $A\beta40_1$ or $A\beta42_1$, respectively, and the surface of soluble Aβ protofibrils, respectively denoted here as $A\beta40_n$ or $A\beta42_n$, are effectively probed at atomic resolution by a combination of ^{15}N T_2 relaxation experiments and selective ^{15}N saturation transfer, as implemented through the dark-state exchange saturation transfer (DEST) NMR pulse sequence (26–31).

Here, we utilize DEST, relaxation, and saturation transfer difference (STD) NMR experiments to monitor the interactions between unlabeled HSA and ^{15}N-labeled Aβ(1–40) and Aβ(1–42). Based on these data, we propose a dual mechanism for the inhibition of Aβ self-association by HSA, whereby at plasma concentrations the latter interacts with both Aβ monomers and protofibrils, targeting key Aβ self-recognition sites and leading to a net switch from direct to tethered contacts between monomeric and protofibrillar Aβ. In this context, the term "tethered" refers to the lack of direct contacts between a given residue of monomeric Aβ and the surface of Aβ protofibrils. Hence, a tethered residue of Aβ monomers is anchored to the Aβ protofibrils through other residues of monomeric Aβ that contact directly the Aβ protofibrils. The relative tethered *versus* direct contact probabilities are residue-specific (26), and the DEST experiment provides a means to quantify these tethered *versus* direct contact probabilities on a residue-specific basis (26). We also show that these HSA-Aβ interactions are isoform-specific, because distinct Aβ(1–40) *versus* Aβ(1–42) differences are observed in the interactions with albumin.

Results

The interaction between monomeric Aβ(1–40) ($A\beta40_1$) and HSA is weak (K_d = ~0.1–1.0 mM) but physiologically relevant

To probe the interactions between HSA and Aβ(1–40) monomers, we analyzed dilute (50–60 μM) solutions of ^{15}N-labeled Aβ(1–40) in both the absence and the presence of equimolar amounts of HSA. Under these dilute conditions, the Aβ(1–40) peptide is primarily monomeric, as supported by the observation of only marginal off-resonance DEST effects and the absence of significant residue-dependent variations (supplemental Fig. S1). No appreciable chemical shift changes are detected for Aβ(1–40) upon addition of HSA (supplemental Fig. S2), consistent with low populations of the high MW $A\beta40_1$–HSA complex relative to free $A\beta40_1$. However, minor fractions of high MW complexes are often sufficient to result in marked enhancements in ^{15}N R_2 rates. Hence, we measured the ^{15}N R_2 relaxation rates of monomeric ^{15}N-labeled Aβ(1–40) with and without equimolar amounts of HSA (Fig. 1*a* and supplemental Fig. S3*b*, *gray bars*).

Fig. 1*a* and supplemental Fig. S3*b* (*gray bars*) reveal that the majority of the significant HSA-induced ^{15}N R_2 enhancements occur within the segments that span the two β-strands (*i.e.* β_1 and β_2) involved in the cross-β structure typical of Aβ fibrils. The largest ^{15}N R_2 increases cluster in the 31–40 region (Fig. 1*a* and supplemental Fig. S3*b*, *gray bars*), suggesting that these C-terminal residues are a primary site for the HSA-$A\beta40_1$ interaction. These results were independently confirmed through STD-HSQC experiments (Fig. 1, *c* and *e*). Fig. 1 (*c* and *e*) reveals that saturation is transferred to multiple $A\beta40_1$ sites, including a continuous stretch spanning residues 30–40, as well as additional residues in the 12–24 region, such as the 17–19 segment in the central hydrophobic core. No major STD-HSQC cross-peaks were observed in the absence of HSA (Fig. 1*c*), confirming that the STD signals observed in the presence of HSA do indeed reflect the transfer of saturation from HSA to Aβ(1–40) and genuinely report on the HSA-$A\beta40_1$ interaction. Overall, the HSA-dependent enhancements in STD and ^{15}N R_2 rates consistently point to the 31–40 C-terminal region in β_2 as a primary consensus site for the binding of $A\beta40_1$ to HSA, with additional interaction sites close to or within the central hydrophobic core of $A\beta40_1$ spanned by β1.

To estimate the K_d value for the HSA-$A\beta40_1$ interaction, a dilute solution of ^{15}N-labeled Aβ(1–40) monomers was titrated with increasing concentrations of HSA, and the titration was monitored through the HSQC intensity losses caused by the HSA-induced R_2 enhancements (Fig. 1*f*). As the HSA concentration increases the signal intensity of several HSQC cross-peaks decreases in a dose-dependent manner (Fig. 1*f*). When the data of Fig. 1*f* are fitted using a Scatchard-like model, K_d values in the 0.1–1.0 mM range are obtained. This result was confirmed by monitoring the binding isotherm through STD/STR ratios (supplemental Fig. S3*c*). However, the exact values of the fitted K_d should be interpreted with caution, because the site-specific affinities (K_d) depend also on the stoichiometry of the $A\beta40_1$–HSA complex. For instance, if only a single molecule of monomeric Aβ(1–40) binds each molecule of HSA (*i.e.* $n = 1$ in Fig. 1*f*), K_d = ~0.2 mM, but if each of the three homologous domains of HSA binds monomeric Aβ(1–40) (*i.e.* $n = 3$ in Fig. 1*f*), then K_d = ~0.6 mM (Fig. 1*f*). Despite these uncertainties, the data of Fig. 1*f* point to HSA binding monomeric Aβ(1–40) with effective K_d values in the 0.1–1.0 mM range, which is comparable with the concentration of HSA in plasma, and suggest that the $A\beta40_1$:HSA interactions, although weak, are physiologically relevant.

Monomeric Aβ(1–42) ($A\beta42_1$) also binds HSA but more weakly than $A\beta40_1$

To investigate whether the ability of plasma albumin to bind $A\beta40_1$ extends to $A\beta42_1$, we repeated the ^{15}N R_2, STD-HSQC, and titration experiments (Fig. 1, *a*, *c*, and *f*) also for dilute solutions of the longer Aβ isoform (Fig. 1, *b*, *d*, and *f*). Fig. 1*b* shows that upon addition of albumin pervasive ^{15}N R_2 relaxation enhancements are observed for most Aβ42 residues, indicating that under our experimental conditions, HSA binds $A\beta42_1$ as well. However, the STD-HSQC and the titration data consistently point to HSA binding $A\beta42_1$ with lower affinity than $A\beta40_1$, despite the longer length of the former peptide (Fig. 1, *d* and *f*). The STD enhancement detected upon addition of albumin to $A\beta42_1$ is marginal (Fig. 1*d*), in stark contrast with the major STD increase observed upon albumin addition to the shorter $A\beta40_1$ under similar experimental conditions (Fig. 1*c*). The reduced STD contribution arising from HSA is consistent with a reduced fraction of albumin-bound peptide in the $A\beta42_1$ *versus* $A\beta40_1$ solutions. Furthermore, the titration data (Fig. 1*f*)

confirm that in going from $A\beta40_1$ to $A\beta42_1$, the site-specific dissociation constant is subject to a ~2-fold increase, resulting in a K_d' value of 450 ± 100 μM, *i.e.* a value that is still non-negligible compared with physiological albumin concentrations in plasma. Based on these affinities and considering a plasma concentration of HSA of 644 μM, significant fractions of albumin-bound monomeric peptide are expected in plasma for both Aβ(1–40) and Aβ(1–42). However, unlike in plasma,

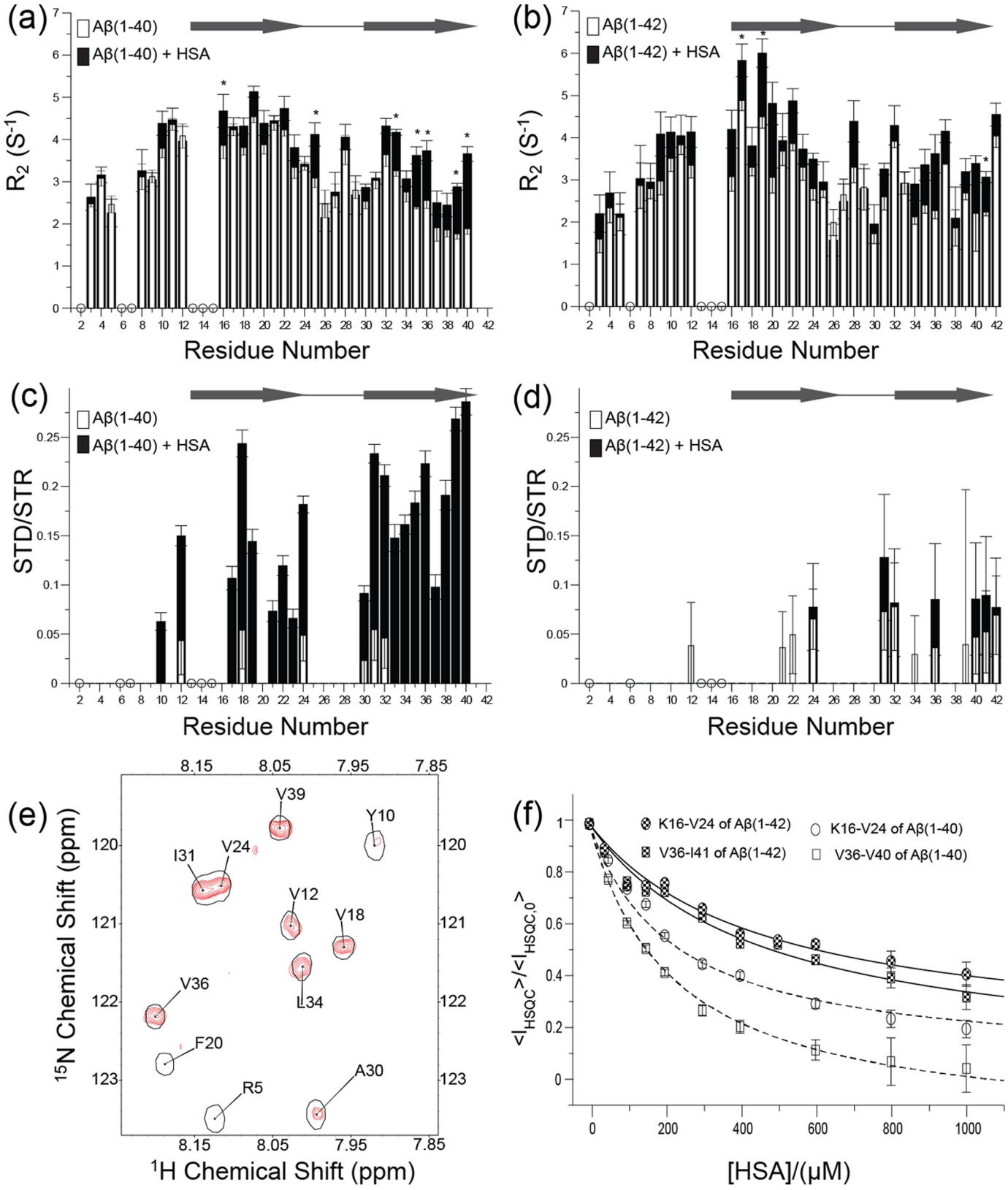

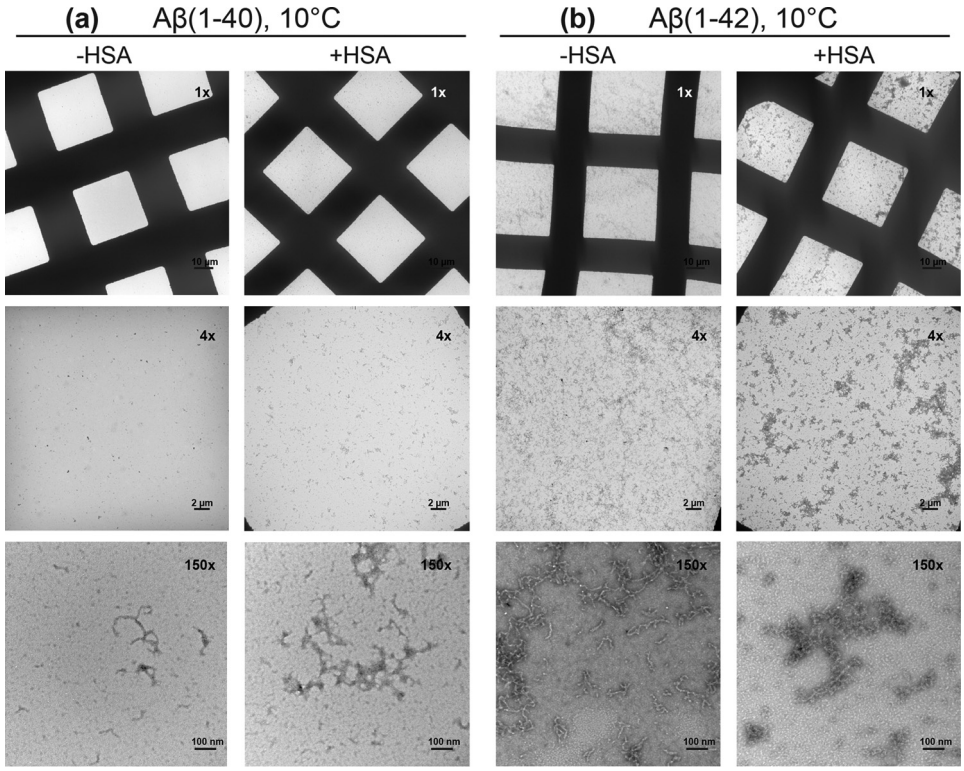

Figure 2. Monitoring Aβ(1–40) and Aβ(1–42) protofibril formation through EM. Negative staining electron micrographs acquired at magnifications of 1,000×, 4,000×, and 150,000×. *a, left panels*: images of 300 μM Aβ(1–40) incubated at 10 °C for 10 days. *a, right panels*: images of 300 μM Aβ(1–40) with 50 μM HSA added at the seventh day of incubation and kept at 10 °C for a total time of 10 days. *b*, as for *a* but using 150 μM Aβ(1–42) ± 30 μM HSA.

HSA concentrations in the CSF are limited to ~3 μM, *i.e.* too low for significant HSA-Aβ_1 interactions but more comparable with the affinity of albumin for Aβ protofibrils (18). Hence, we proceeded to investigate the effect of HSA on more concentrated solutions of Aβ(1–40) and Aβ(1–42), in which Aβ monomers are in a dynamic pseudo-equilibrium with Aβ assemblies.

Preparation of Aβ(1–40) and Aβ(1–42) protofibrils (Aβ40$_n$ and Aβ42$_n$)

To examine the effect of HSA on the Aβ monomer-protofibril exchange process, we prepared a concentrated (300 μM) solution of ^{15}N-labeled Aβ(1–40). Aβ peptides are known to form large amyloid protofibrils spontaneously when dissolved at concentrations higher than 100 μM (26). If incubated at 37 °C in the absence of albumin, the Aβ(1–40) protofibrils grow into large fibrils, as shown by EM images at 150,000× magnification (supplemental Fig. S4, *left panels*), which form highly compact and dense tangles, as shown by EM images at 1,000–4,000× magnification (supplemental Fig. S4, *left panels*). However, when the concentrated Aβ(1–40) sample is left to equilibrate at low temperature (4–10 °C) for 7–10 days, a pseudo-equilibrium is reached in which Aβ monomers are in dynamic exchange with protofibrils (Aβ40$_n$) (26). Indeed, after 10 days of incubation at 10 °C, our 300 μM Aβ(1–40) solution contained large (>10 nm) worm-like aggregates, as shown by dynamic light scattering (supplemental Fig. S5*a*) and electron microscopy (Fig. 2*a*, *left panels*). Unlike the results obtained at higher temperatures (supplemental Fig. S4, *left panels*), which serve as our positive control, the Aβ(1–40) sample at 10 °C did not contain any observable fibrillar tangles or mature fibers (Fig. 2*a*, *left panels*). Similar conclusions were reached also for the preparation of Aβ(1–42) protofibrils (Aβ42$_n$) at 10 °C, as supported by DLS (supplemental Fig. S6) and EM data (Fig. 2*b*,

Figure 1. Binding of HSA to Aβ(1–40) and Aβ(1–42) monomers as monitored by ^{15}N R_2 relaxation, ^{1}H saturation transfer, and HSQC intensity changes. *a*, ^{15}N-R_2 relaxation rates of 60 μM Aβ(1–40), which is mostly monomeric, in the absence of HSA (*white bars*) and in the presence of equimolar amounts of HSA (*black bars*). *b*, as in *a*, but for 50 μM Aβ(1–42). *Asterisks* in *a* and *b* denote statistical significance with $p < 0.05$. *c*, ^{1}H saturation transfer of 40 μM Aβ(1–40) in the absence (*white bars*) and presence of 200 μM HSA (*black bars*). Saturation transfer was quantified as the residue-specific ratios between the STD and the saturation transfer reference (*STR*) intensities. *d*, as in *c*, but for 40 μM Aβ(1–42) in the absence and presence of 200 μM HSA. The *gray arrows* in *a* and *c* and in *b* and *d* denote the proposed position of β-strand regions in Aβ(1–40) and Aβ(1–42) fibrils (26), respectively. The *open circles* in *a–d* flag ambiguous residues caused by overlap and/or line broadening. *e*, representative expansion of the STD-HSQC spectrum used in *c* (*red cross-peaks*) superimposed to the corresponding STR-HSQC cross-peaks (*black single contours*). *f*, titration of HSA into a solution of 40 μM ^{15}N-labeled Aβ(1–40) monitored through HSQC intensity losses quantified as the $<I_{HSQC}>/<I_{HSQC,0}>$ ratio (*open symbols* and *dashed fitted lines*). $<I_{HSQC}>$ is the average signal intensity for either residues Val^{36}–Val^{40} (*open squares*) or residues Lys^{16}–Val^{24} (*open circles*), after correction for dilution effects. These regions were selected because they are most affected by HSA. $<I_{HSQC,0}>$ denotes the $<I_{HSQC}>$ value measured in the absence of HSA. The data were fitted using a Scatchard-like model (*dashed lines*), which represents one of the simplest models of binding (see "Experimental procedures"). For Aβ(1–40), the data are consistent with a site-specific dissociation constant $K_d = (220 \pm 50\ \mu M)*n$, where n is the number of independent and equivalent binding sites for the monomeric Aβ peptide within HSA. If each homologous domain of HSA binds monomeric Aβ(1–40), then $n = 3$. A similar analysis was extended to Aβ(1–42) (*filled symbols* and *solid fitted lines*), resulting in a site-specific dissociation constant $K_d = (450 \pm 100\ \mu M)*n$. Again, if each homologous domain of HSA binds monomeric Aβ(1–42), then $n = 3$.

left panels), and of Aβ(1–42) fibrillar tangles at 37 °C (supplemental Fig. S7, *left panels*).

The presence of protofibrils in dynamic exchange with NMR-visible Aβ monomers in concentrated Aβ(1–40) samples was independently confirmed by the average difference in NMR ^{15}N transverse relaxation rates (ΔR_2) between the 300 μM and the diluted 60 μM Aβ(1–40) reference solution, which is greater than 1.00 s^{-1} (*i.e.* ~1.45 s^{-1}, supplemental Fig. S8*A*), as expected for NMR-invisible ("dark") Aβ(1–40) protofibrils (32). The maximum value of ΔR_2 provides an estimate of the pseudo first-order rate constant $k_{on,\,app}$ for the conversion from NMR-visible to invisible species (26), which based on supplemental Fig. S8*A* is ~2 s^{-1}. We then investigated how this dynamic steady state Aβ40$_1$-Aβ40$_n$ exchange is affected by HSA.

An approach to probe how HSA perturbs the Aβ monomer-Aβ protofibril interactions: the Θ values

The ΔR_2 *versus* residue profile measured for concentrated (>100 μM) Aβ samples is typically combined with DEST data from ^{15}N-selective saturation experiments at multiple offsets to map the Aβ40$_1$-Aβ40$_n$ interactions (26). The combined analysis of the ΔR_2 and DEST profiles provides a residue-specific constant, defined as K_3, which quantifies the partitioning of a given Aβ residue *i* between direct and tethered contacts with the Aβ protofibril surface. However, this quantitative approach requires highly precise DEST measurements with ^{15}N-selective saturation at multiple offset frequencies and hence long acquisition times during which the pseudo-equilibrium of Aβ solutions may change, thus biasing the comparisons with the data acquired in the presence of HSA. As a first step toward minimizing this experimental bias and reducing the DEST acquisition time, while still probing how HSA perturbs the Aβ monomer-protofibril equilibrium, we analyzed the DEST data similarly to the analysis of the traditional ^{1}H STD experiments. Specifically, we calculated the DEST difference (Θ), or single point DEST, which is defined here according to the following equation,

$$\Theta = \frac{\sum \pm I^{\circ} - \sum \pm Ist}{\sum \pm I^{\circ}} \qquad \text{(Eq. 1)}$$

where I° refers to the DEST intensities measured at far off-resonance ^{15}N frequency offsets (*e.g.* ± 35 kHz), which serve as a reference, whereas *Ist* refers to the DEST intensities measured at ^{15}N frequency offsets sufficiently close to the carrier frequency ("near off-resonance offsets") to saturate Aβ protofibrils but still sufficiently far from the ^{15}N resonance frequencies of monomeric Aβ to minimize direct saturation of Aβ monomers (*e.g.* ± 2–8 kHz). The Σ± notation indicates that the intensities at the positive and negative offset values were averaged to remove to first order the effect of the ^{15}N chemical shift resonance offset on the on single point DEST (Θ). The single point DEST (Θ) reports primarily on the width of the DEST intensity *versus* ^{15}N-saturation offset profile and is expected to range between 0 and 1, with the former (latter) value approached by Aβ monomers residues subject to primarily tethered (direct) contacts with the surface of the Aβ protofibrils.

To test the effectiveness of the proposed single point DEST (Θ) method in probing the Aβ40$_1$-Aβ40$_n$ interactions, we computed the Θ values using previously acquired Aβ(1–40) DEST data, for which the K_3 direct *versus* tethered contact partitioning coefficients were determined through the combined McConnell fitting of DEST and R_2 data (32). The Θ values were computed utilizing DEST intensities measured with a 350 Hz ^{15}N saturating field strength at three different offset pairs differing in the near off-resonance values: {±35 kHz, ±2 kHz}, {±35 kHz, ±4 kHz}, and {±35 kHz, ±8 kHz}, as shown in supplemental Fig. S9*a*. Supplemental Fig. S9*a* shows that the Θ *versus* residue profiles calculated using different near off-resonance values, *i.e.* ±2 kHz, ±4 kHz, and ±8 kHz, exhibit similar patterns, with maxima located at similar residue numbers. Given these similarities, we opted for ±4 kHz as the optimal near off-resonance saturation frequency, because it provides the advantage of a balanced compromise between adequate saturation of the Aβ protofibrils, resulting in significant cross-peak attenuation (up to ~40%, supplemental Fig. S9*a*) and optimal Aβ protofibril *versus* monomer selectivity (32). The minimal effect of the selective ^{15}N saturation at ±4 kHz on the Aβ monomer is proven by the negligible magnitude of the Θ values measured for a dilute (60 μM) solution of primarily monomeric Aβ(1–40) (supplemental Fig. S1, *black bars*).

To test the suitability of Θ values at ±4 kHz to estimate the K_3 values, we compared the residue profiles for both Θ and K_3 as shown in supplemental Fig. S9*b*. The Θ *versus* K_3 comparison (supplemental Fig. S9*b*) indicates that the two parameters exhibit similar trends, with both profiles featuring maxima at similar residue positions. Hence, the Θ residue profile provides an approximation to the relative K_3 values, as required to effectively probe the effect of HSA on Aβ protofibrils.

Next, we checked to what extent the Θ parameter is field-dependent. For this purpose, the single point DEST (Θ) was measured at ±4 kHz and 700 MHz for a concentrated (300 μM) Aβ(1–40) solution equilibrated for 7 days at 4 °C and compared to those computed using the published data acquired for a similar Aβ (1–40) sample at ±4 kHz and 900 MHz (18, 23) (supplemental Fig. S9*c*). Despite the difference in field, and consequently in relative offsets as well, the two plots in supplemental Fig. S9*c* exhibit overall similar relative trends with two maxima centered at residues ~18 and ~33, consistently showing that the N-terminal residues prefer tethered states, whereas the central hydrophobic core and part of the C-terminal residues are more likely to be engaged in direct contacts with the protofibril surface.

The single point DEST (Θ) profiles reveal that HSA promotes a switch from direct to tethered-contacts for the Aβ(1–40) residues involved in protofibril growth

The Θ profile was measured again after adding 70 μM of unlabeled HSA to the equilibrated 300 μM ^{15}N-labeled Aβ(1–40) solution. With the exception of the worm-like aggregates becoming slightly more electron dense in the presence of HSA, the addition of HSA did not result in any major change in the protofibril integrity as monitored by DLS (supplemental Fig. S5) and EM (Fig. 2*a*) under our experimental conditions. However, significant changes in Θ values were observed for most Aβ

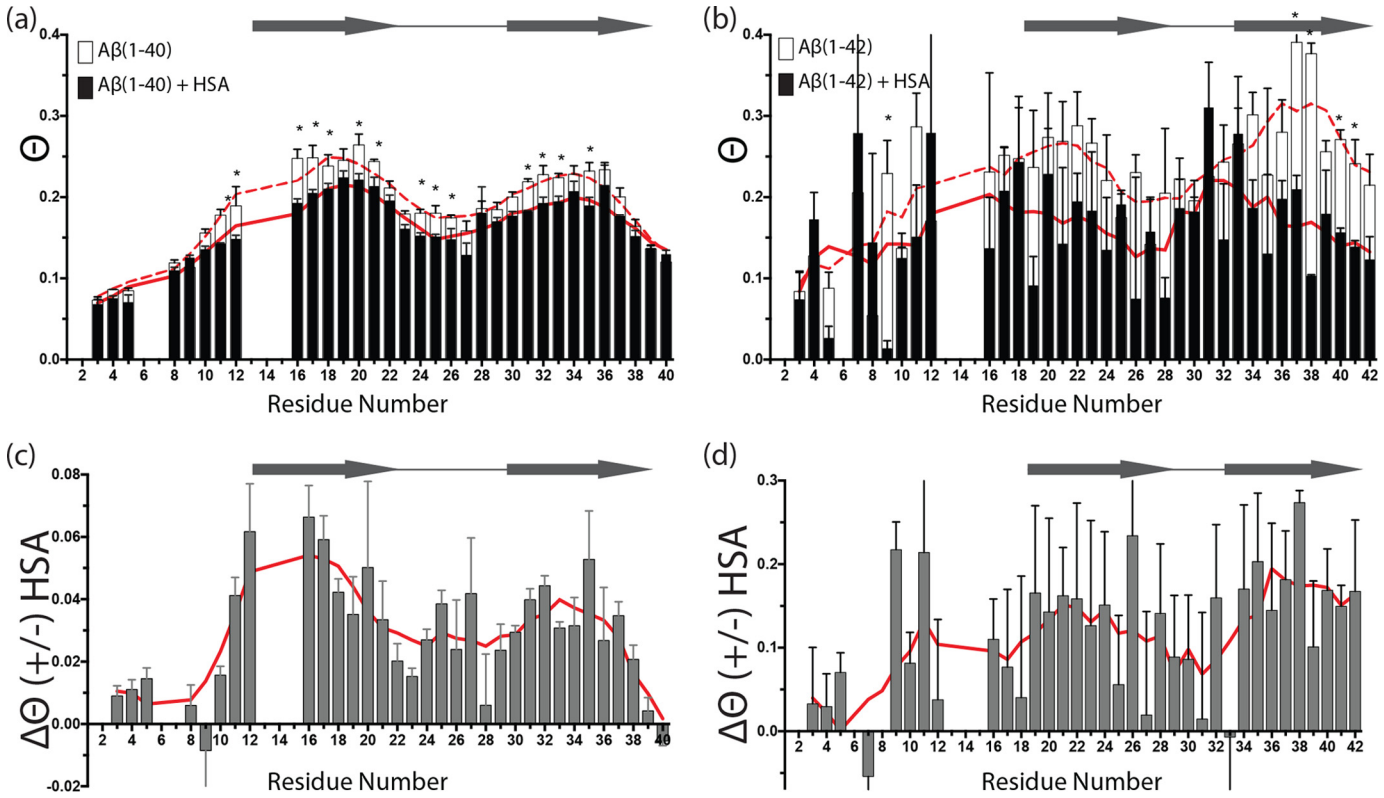

Figure 3. Effect of HSA on the single point DEST (Θ) profiles of concentrated Aβ(1–40) and Aβ(1–42) in a dynamic pseudo-equilibrium state between monomers and protofibrils (dark state). *a*, Θ values for 300 μM Aβ(1–40) in the absence (*white bars*) and presence (*black bars*) of 70 μM HSA. *b*, Θ values for 150 μM Aβ(1–42) in the absence (*white bars*) and presence (*black bars*) of 50 μM HSA. *c* and *d*, residue-specific differences between the two Θ profiles of *a* and *b*, respectively. In *a* and *b*, *smoothed lines* in the absence (*dashed red line*) and presence of HSA (*solid red line*) are displayed behind the bars, whereas *smoothed lines* are displayed as *solid red lines* in *c* and *d*. *Smoothed lines* were calculated by averaging Θ values between the measured Θ value of one residue and those for the two amino acids adjacent to it, when available. *Horizontal arrows* and *empty circles* have the same meaning as in Fig. 1. The data are means of 2–3 replicates ± S.E. *a* and *b* were analyzed for statistical significance using a Student's *t* test. *Asterisks* denote statistical significance with $p < 0.05$.

residues (Fig. 3*a* and supplemental Fig. S11), consistent with an overall perturbation of the direct *versus* tethered Aβ(1–40) monomer-protofibril contact distribution arising from interactions of HSA with $Aβ40_n$ and possibly with $Aβ40_1$.

The contribution of free HSA-$Aβ40_1$ complexes to the HSA-dependent Θ changes observed in Fig. 3*a* is expected to be negligible based on two main lines of evidence. First, under the experimental condition of Fig. 3, the fraction of $Aβ40_1$ bound to HSA is minimal because of its weak affinity. Second, when unlabeled HSA is added to a dilute solution of ^{15}N-labeled $Aβ40_1$, no significant changes were observed in the DEST profile (supplemental Fig. S1). These observations suggest that the HSA-dependent Θ changes observed in Fig. 3*a* arise mainly from direct interactions between HSA and the $Aβ40_n$ protofibrils, which bind albumin with higher affinity than Aβ(1–40) monomers (10, 18). Hence, the residue-specific Θ variations caused by HSA (Fig. 3, *a* and *c*) are a valuable indicator of how HSA binding to $Aβ40_n$ affects the direct *versus* tethered contact partitioning of Aβ(1–40) monomers at the surface of the $Aβ40_n$ protofibrils provided that contributions from changes in $k_{on,\,app}$ or the populations of protofibrils are ruled out (as explained in the next section).

As shown in Fig. 3 (*a* and *c*), the Θ values for the majority of Aβ(1–40) residues are decreased in the presence of HSA (Table 1), with the most significant Θ reductions observed for the central hydrophobic core and the region preceding the C terminus,

Table 1
DEST data statistics

	Aβ (1–40)	Aβ (1–42)
$<Θ>^a$	0.19 ± 0 .01	0.21 ± 0 .05
$<ΔΘ\ (+/-)\ HSA>^b$	0.03 ± 0 .01	0.08 ± 0 .04

[a] Based on the data of Fig. 3 (*a* and *b*).
[b] Based on the data of Fig. 3 (*c* and *d*). The ΔΘ value depends on HSA concentration as shown in supplemental Fig. S11.

at or near the in-register β-sheets of the protofibril structure. Only minimal or negligible differences were observed for the N terminus and the very C-terminal residues (Fig. 3, *a* and *c*). The decrease in Θ values observed upon HSA addition suggests that HSA promotes a switch from direct to tethered contacts between the $Aβ40_1$ monomers and the $Aβ40_n$ protofibril surface. These results were independently confirmed at physiological temperature (37 °C) by acquiring DEST data both in the absence and presence of albumin (supplemental Fig. S10). Supplemental Fig. S10 shows that incubation at 37 °C for 24 h of a dilute Aβ(1–40) sample results in a significant DEST effect for both β1 and β2 regions only in the absence of albumin, confirming that HSA leads to a switch from direct to tethered contacts between Aβ(1–40) monomers and protofibrils. In addition, our EM data at 37 °C (supplemental Fig. S4, 1,000× and 4,000× magnification images, *right panels*) suggest that albumin causes the fibril clumps to become more loosely packed than those observed in the absence of HSA. The EM images at

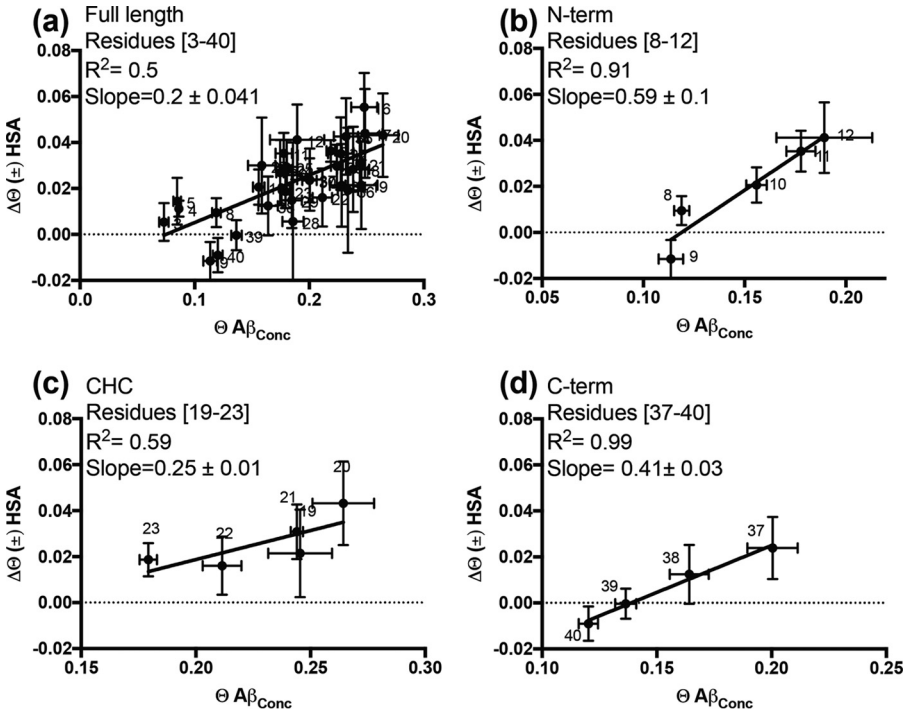

Figure 4. Correlation between the Θ changes caused by HSA addition (ΔΘ (±) HSA) and the dark Θ values measured in the absence of HSA. *a*, correlation for the full-length Aβ(1–40) peptide. *b–d*, correlations for selected segments of Aβ(1–40): 8–12, 19–23, and 37–40, respectively. Assuming Θ values become null at infinite dilution, the dark Θ values reported on the *horizontal axis* represent the Θ value variations occurring upon dilution in the absence of albumin, *i.e.* the ΔΘ Aβ(1–40) dilution values.

150,000× magnification also show that HSA coats the Aβ fibrils (supplemental Fig. S4, *right panels*), explaining the direct-to-tethered switch for the $A\beta40_1$-$A\beta40_n$ contacts observed by DEST (supplemental Fig. S10).

To probe to what extent the switch from direct to tethered contact states promoted by HSA resembles that caused by the spontaneous release of $A\beta40_1$ from $A\beta40_n$ protofibrils, we compared the Θ change measured upon HSA addition to the concentrated 300 μM Aβ(1–40) sample (*i.e.* ΔΘ (±) has in Fig. 4) to the Θ change observed upon dilution of the concentrated (300 μM) Aβ(1–40) sample in the absence of HSA, *i.e.* Θ for concentrated Aβ(1–40) assuming negligible Θ values at infinite dilution (Fig. 4). When all Aβ(1–40) residues are included in the comparison, the ΔΘ (±) HSA and the Θ values for concentrated Aβ(1–40) appear poorly correlated (Fig. 4*a*). However, when the ΔΘ analysis is confined to selected Aβ(1–40) segments, such as residues toward the N terminus (*i.e.* 8–12) and residues that span the C-terminal region, *i.e.* 37–40, a higher degree of correlation is observed (Fig. 4, *b* and *d*), suggesting that in these regions the effect of HSA addition is more comparable to that of Aβ dilution. Interestingly, the slopes of the correlations are different in the two segments (Fig. 4, *b* and *d*), showing that the extent of the dilution-like effect of HSA is region-specific.

Effect of HSA on the $k_{on,\ app}$ or the populations of protofibrils

It should also be considered that a decrease in the Θ value might result from a reduction not only in K_3, but also in $k_{on,\ app}$ and/or the total population of protofibrils. To assess the contributions from the latter two parameters, it is important to evaluate the dark *versus* dilute R_2 change (ΔR_2) also in the presence of HSA. In fact, $k_{on,\ app}$ typically equates the maximum value of ΔR_2 (26). To obtain the dark *versus* dilute ΔR_2, we corrected for the R_2 contributions arising from the binding of HSA to Aβ(1–40) monomers by estimating the amount of Aβ(1–40) monomers in the dark samples through HSQC intensity losses over time (*i.e.* 144 μM; supplemental Fig. S12). In addition, the concentration of HSA available to interact with monomeric Aβ(1–40) is not expected to be significantly different from the total concentration of HSA in the dark sample, 70 μM HSA. Based on the measured affinity (Fig. 1*f* and supplemental Fig. S3*c*) at 144 μM monomeric Aβ(1–40) and 70 μM HSA, the fraction of albumin-bound Aβ(1–40) monomers is expected to be ~17%, which matches quite closely the fraction of albumin bound Aβ(1–40) monomers in the sample with 60 μM monomeric Aβ(1–40) and 60 μM HSA used for the measurement of R_2 rates in Fig. 1*a* (*i.e.* ~18%). The R_2 rates of Fig. 1*a* (*solid black bars*) were then subtracted from the respective R_2 values measured for the dark sample in the presence of 70 μM HSA to obtain the ΔR_2 plot corrected for the R_2 contributions arising from the binding of HSA to Aβ(1–40) monomers (supplemental Fig. S8*a*, *filled black bars*). The comparison of the corrected dark *versus* dilute ΔR_2 profiles in the presence *versus* absence of HSA (supplemental Fig. S8*a*, *filled versus open bars*) reveals two important points.

First, supplemental Fig. S8*a* shows that, if decreases in $k_{on,\ app}$ and/or the total population of protofibrils occur upon addition of HSA, they are sufficiently limited to result in ΔR_2 changes that fall within the experimental error margin of our R_2 data, *i.e.* HSA does not significantly decrease the ΔR_2 values (supplemental Fig. S8*a*). Second, supplemental Fig. S8*a* reveals that,

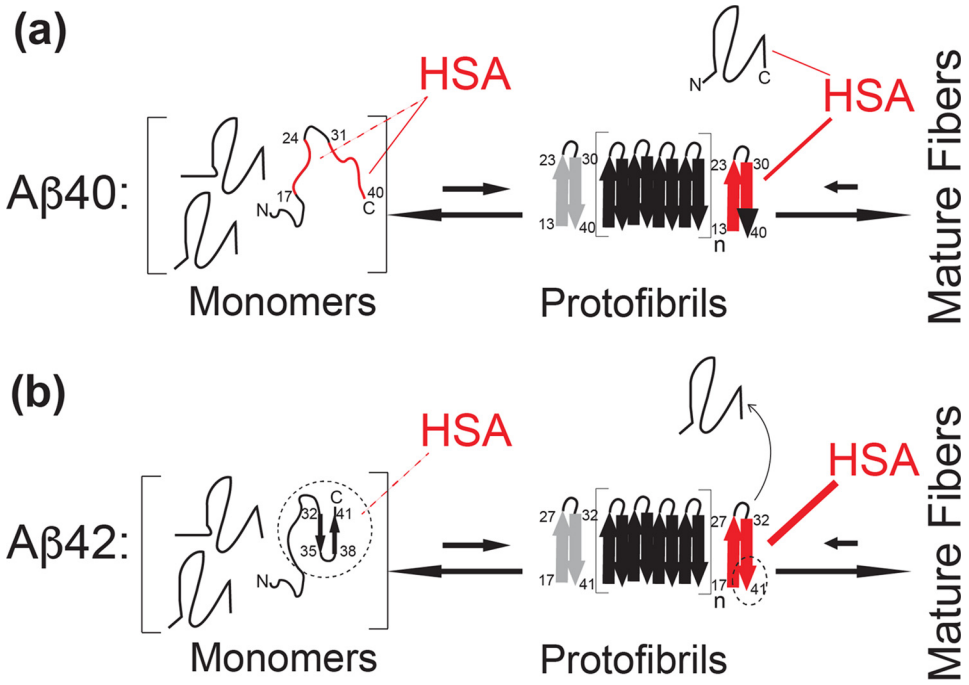

Figure 5. Schematic model for the mechanism of Aβ(1–40) *versus* Aβ(1–42) self-association inhibition by HSA. Key Aβ regions affected by HSA are shown in *red*. *a*, model of Aβ(1–40)- HSA interactions. HSA binds weakly (K_D = ~0.1–1 mM) to the largely unstructured Aβ(1–40) monomers targeting primarily the C-terminal 31–40 residues (*solid red line*), as well as a secondary site spanning residues 17–24 (*dashed red line*). HSA also binds Aβ(1–40) protofibrils with higher affinity than Aβ(1–40) monomers ($Aβ40_1$) and competes with the direct contacts between $Aβ40_1$ and the Aβ(1–40) protofibrils, thus inhibiting further growth into mature fibers that would otherwise occur under non-pseudo-equilibrium conditions in the absence of HSA, as explained in the text. However, HSA may also mediate indirect contacts between the $Aβ40_1$ and the Aβ(1–40) protofibrils. The Aβ(1–40) residues involved in fibril cross-β structures are represented by *thick arrows* (23, 47, 48). One edge of the protofibril is displayed in *gray* to denote that HSA may not interact with both edges (12). *b*, model of Aβ(1–42)- HSA interactions. The last two residues of Aβ(1–42) stabilize a C-terminal turn in the monomeric peptide, possibly shielding the C-terminal region from HSA and reducing the affinity of Aβ(1–42) monomers for HSA (*dashed thin line* rather than *solid thick red line*). However, the last two residues of Aβ(1–42) also promote extensive HSA-induced protofibril perturbations (*thicker red line*), which now reach the C-terminal region of the second β-strand (full *red* rather than *red/black C-terminal arrow*). The *black dashed circles/ovals* highlight the sites of the Aβ(1–40) *versus* Aβ(1–42) differences.

even after correction for the binding of free HSA to residual monomeric Aβ(1–40) in the dark sample, a significant ΔR_2 enhancement is observed upon HSA addition for several residues, especially in the C-terminal region (*e.g.* residues 37–40, supplemental Fig. S8*a*). This interesting effect is consistent with Aβ(1–40) monomers interacting with protofibril-bound HSA and with the presence of multiple homologous domains in HSA. For example, although one domain of HSA binds the Aβ(1–40) protofibrils, another domain of HSA may recruit Aβ(1–40) monomers, which interact with albumin primarily through the C-terminal residues, as shown in Fig. 1 (*a*, *c*, and *f*). This example illustrates how Aβ(1–40) monomers can interact with the Aβ(1–40) protofibrils not only through direct contacts with the protofibril surface but also through indirect contacts mediated by protofibril-bound HSA.

The HSA-induced switch from direct to tethered contacts is Aβ isoform-specific

To test to what extent the albumin-induced remodeling of the direct *versus* tethered contacts observed for Aβ(1–40) is isoform-specific, we extended the comparative DEST Θ analyses to Aβ(1–42) (Fig. 3*b*). Fig. 3*b* reveals that, similarly to Aβ(1–40), also for Aβ(1–42) albumin induces a pervasive reduction in Θ values (Table 1), without major perturbations of the morphology of the Aβ protofibrils in solution as supported by DLS (supplemental Fig. S6*b*) and EM data (Fig. 2*b*), except for the worm-like aggregates becoming more electron dense in the samples with HSA. However, the ΔR_2 values for Aβ(1–42) (supplemental Fig. S8*b*) reveal that the interpretations of the albumin-induced ΔΘ profiles of Aβ(1–40) and Aβ(1–42) (Fig. 3, *c* and *d*) are markedly different. Unlike for Aβ(1–40), for Aβ(1–42) a reduction of ΔR_2 is observed upon addition of HSA, suggesting that in this case HSA may act simply by reducing the effective $k_{on,\ app}$ and/or the total population of protofibrils. Furthermore, in the case of Aβ(1–42), no evidence is observed for HSA-mediated contacts between Aβ(1–42) monomers and protofibrils, consistent with the weaker interactions between Aβ(1–42) monomers and albumin, as per Fig. 1. Another clear Aβ(1–42) *versus* Aβ(1–40) difference is that in the case of Aβ(1–42), the HSA-induced Θ reduction extends to the C-terminal residues (Fig. 3*d*), whereas for Aβ(1–40), the effect of HSA on the last five residues progressively decreases to negligible values for the last two residues (Fig. 3*c*).

Discussion

Our main findings are summarized in the scheme shown in Fig. 5. Fig. 5*a* illustrates that Aβ(1–40) interacts with HSA through a dual binding mechanism involving both Aβ(1–40) monomers and protofibrils. The former Aβ(1–40) species are bound by HSA with K_d values in the 0.1–1.0 mM range, whereas the latter bind albumin with affinities higher by ~2–3 orders of magnitude, typically in the ~ μM range (9, 11). Hence, in plasma, where the physiological concentration of HSA is ~0.6–0.7 mM (3), albumin is expected to interact with both Aβ(1–40)

monomers and protofibrils, whereas in the CSF, where the concentration of HSA is ~3 μM (3), only the HSA-Aβ(1–40) protofibril interactions are anticipated to be physiologically relevant.

An unprecedented picture of how HSA perturbs the Aβ(1–40) protofibrils is provided by the residue-resolution single-point DEST (Θ) profiles (Fig. 3, *a* and *c*). Our results show that the HSA-A$\beta40_n$ interactions affect preferentially Aβ(1–40) residues involved in protofibril cross-β strand growth and promote a switch of these Aβ(1–40) monomer-protofibril contacts from a direct to a tethered state (Fig. 5*a* and 3*b* and supplemental Fig. S10). For residues in the 8–12 and 37–40 regions, the ΔΘ values arising from the HSA-induced direct-to-tethered switch correlate with the corresponding ΔΘ values observed upon dissociation of Aβ(1–40) protofibrils into monomers (Fig. 4, *b* and *d*). These observations point to HSA shielding the protofibril at the sites of cross-β strand growth and competing with further Aβ(1–40) monomer addition to the protofibrils (Fig. 5*a*), thus inhibiting protofibril growth into mature Aβ(1–40) fibrils, as confirmed by our EM data (supplemental Fig. S4). However, the lack of global correlations between the effects of dilution and HSA addition on Θ (Fig. 4*a*) suggests that HSA does not simply act by completely shielding Aβ(1–40) protofibrils from Aβ(1–40) monomers. Additional effects are likely present, such as binding of HSA to a subtype of protofibrils or protofibril-binding sites or HSA-mediated contacts between Aβ(1–40) protofibrils and Aβ(1–40) monomers.

In plasma, a further contribution to the inhibition of Aβ(1–40) protofibril growth is provided by the albumin-Aβ(1–40) monomer (A$\beta40_1$) interactions, which affect multiple residues in the two β-strands involved in Aβ(1–40) self-recognition, similarly to the albumin-Aβ(1–40) protofibril (A$\beta40_n$) interactions (Fig. 5*a*). However, our data also reveal distinct differences between the interactions of HSA with A$\beta40_n$ and A$\beta40_1$. In the case of the latter species, a key site for binding with HSA is the C-terminal region of Aβ(1–40) (*i.e.* 31–40), as confirmed by HSA-induced ^{15}N R_2 and ^{1}H STD enhancements that progressively increase in going from residue 37 to 40 (Fig. 1*c*). On the contrary, in the case of A$\beta40_n$, the albumin-induced Θ variations observed at the C-terminal region of A$\beta40_n$ progressively decrease in going from residues 37 to 40 (Fig. 3*c*). In this respect, the interactions of HSA with A$\beta40_1$ appear to complement those with A$\beta40_n$ (Fig. 5*a*), and together they provide an exhaustive and efficient coverage of the Aβ(1–40) residues in both β-strands of the cross-β fibrils, which fully span both the central hydrophobic core and the C-terminal region (Fig. 5*a*), rationalizing the high anti-amyloidogenic potency of albumin in plasma (2, 3).

The balance between Aβ monomer *versus* protofibril interactions with HSA is subject to marked changes in going from the Aβ(1–40) to the Aβ(1–42) isoform (Fig. 5*b*). The Aβ(1–42) monomers bind HSA more weakly than Aβ(1–40) monomers primarily because of a loss of interactions in the C-terminal region (Figs. 1 and 5*b*). A possible explanation for this observation is the stabilization by residues Ile^{41} and Ala^{42} of a C-terminal turn centered at Gly^{37} and Gly^{38} in monomeric Aβ(1–42) (33–45) (Fig. 5*b*). To the extent that these intramolecular Aβ(1–42) interactions compete with HSA binding, they account for the reduced HSA affinity for A$\beta42_1$ *versus* A$\beta40_1$. However, the loss of C-terminal interactions with HSA at the level of Aβ(1–42) monomers is compensated by an enhanced effect of HSA on the C-terminal contacts in the Aβ(1–42) protofibrils (Fig. 3). Unlike Aβ(1–40), in the case of Aβ(1–42), the HSA-induced shift from direct to tethered contacts extends to the very C-terminal residues (Figs. 3*d* and 5*b*).

In summary, for both Aβ(1–40) and Aβ(1–42), the HSA interactions of the C-terminal Aβ region relies on a monomer *versus* protofibril compensation strategy; however, the relative monomer *versus* protofibril balance is Aβ isoform-specific. In the case of Aβ(1–40), the C-terminal Aβ segment mediates primarily the HSA-Aβ monomer interactions, whereas in the case of Aβ(1–42), the C-terminal Aβ segment is perturbed primarily by the HSA-Aβ protofibril interactions (Fig. 5). Overall, the model emerging from our data (Fig. 5) provides a framework to understand the physiological role of HSA as an endogenous anti-Aβ amyloid agent in the CSF and plasma. In addition, the mechanism of Fig. 5 also addresses and clarifies previous discrepancies about the affinities of albumin for Aβ monomers *versus* protofibrils.

The approximately submillimolar affinity range proposed here based on our NMR data (Fig. 1*f*) is in agreement with previous surface plasmon resonance results indicating that monomeric Aβ(1–40) did not lead to detectable binding to HSA at 25 μM concentrations, irrespective of how monomeric Aβ(1–40) was immobilized on the sensor chip, *i.e.* through monoclonal antibodies or streptavidin (3). However, K_d values in the submillimolar range are markedly higher than previously reported μM affinities between Aβ(1–40) monomers and HSA based on low-resolution techniques, such as CD and immunoassays (13, 46–48). This apparent discrepancy is explained considering that previous determinations of Aβ(1–40)- HSA affinities (46, 47) may reflect also contributions from Aβ(1–40) oligomers, which are known to bind HSA more tightly than Aβ(1–40) monomers (9, 11). This interpretation is corroborated by a recent surface plasmon resonance investigation showing that early Aβ oligomers in equilibrium with monomers are sufficient to lower the effective measured K_d value to the μM range (18). In addition, the presence of Aβ(1–40) oligomers is supported by the observation that the binding isotherm built using CD data leads to Hill coefficients significantly greater than 1 (1.4–1.5) (46), which cannot be explained simply by the 1:1 binding of HSA and Aβ(1–40) monomers. Furthermore, contributions to the CD spectra from both Aβ(1–40) and HSA are not easily deconvoluted, whereas this problem is solved here by selectively ^{15}N-labeling Aβ(1–40), but not HSA (supplemental Fig. S2), and by using NMR approaches that directly report on monomer interactions. Overall, our data on both monomeric Aβ(1–40) and Aβ(1–42) rule out that HSA binds the monomeric forms of these Aβ peptides with approximately micromolar K_d values and are consistent with affinities lower by ~2 orders of magnitude, in the submillimolar range (Fig. 1*f*).

Conclusions

Our data indicate that the inhibition of Aβ(1–40) self-association by HSA relies on a dual mechanism, whereby at plasma

concentrations albumin binds both Aβ(1–40) monomers and protofibrils, targeting key Aβ(1–40) self-recognition sites and triggering a net switch from direct to tethered contacts between monomeric and protofibrillar Aβ (Fig. 5). We also show that in going from the Aβ(1–40) to Aβ(1–42) isoform, the engagement of the C-terminal Aβ residues increases at the level of the Aβ protofibril-HSA contacts but decreases at the level of Aβ monomer-HSA interactions, which become weaker. These results provide an unprecedented view of the mechanism underlying the Aβ self-association by albumin. In addition, they also demonstrate the potential of a general NMR approach to probe at residue resolution how amyloid inhibitory proteins perturb Aβ self-association. Inhibitor-induced enhancements in ^{15}N R_2 rates and in ^{1}H STD-HSQC ratios unveil the sites of Aβ monomer interactions, whereas inhibitor-dependent changes in DEST under dark conditions, quantified as variations in the Θ observable, identify the Aβ protofibril residues affected by the inhibitor and, when combined with the analysis of dark *versus* dilute R_2 changes corrected for monomer interactions, provide a quantitative measure of how the inhibitor perturbs the direct *versus* tethered partitioning of the Aβ monomer-protofibril contacts. Hence, the DEST method (26) was essential to elucidate the inhibitory mechanism proposed here (Fig. 5).

Experimental procedures

Sample preparation

Peptide solutions were prepared as previously described (42). In brief, the Aβ(1–40) or Aβ(1–42) peptides (rPeptides Inc.) were dissolved in 3 mM NaOH at a concentration of 1 mg/ml and a pH adjusted to 11 using a 50 mM NaOH solution. Peptide solutions were then divided into different aliquots containing enough Aβ peptides to obtain 500-μl final solutions at the desired Aβ peptide concentrations, *i.e.* 40–60 and 300 μM for dilute and dark Aβ(1–40) samples, respectively, and 40–50 and 150 μM for dilute and dark Aβ(1–42) samples, respectively. The aliquots were freeze-dried, and the lyophilized powder of each aliquot was resolubilized using 250 μl of 3 mM Tris-HCl, pH 8.0, and buffer-exchanged with a Zeba desalting column pre-equilibrated with Tris buffer. Desalted solutions were adjusted to 50 mM HEPES buffer, 10% D_2O, pH 6.8, by the addition of 250 μl of 100 mM HEPES buffer, 20% D_2O, pH 6.3, and up to additional 30 μl of 100 mM HEPES buffer, pH 6.8, as necessary to fine tune the pH. A 1 mM HSA stock solution was prepared by dissolving lyophilized HSA, essentially fatty acid, and globulin free (A3782; Sigma), in 50 mM HEPES buffer, 10% D_2O, pH 6.8. All solutions were treated with a chelating agent (Chelex 100; Sigma-Aldrich) to remove any residual metals. In all experiments involving concentrated Aβ samples (*i.e.* 300 μM Aβ(1–40) or 150 μM of Aβ(1–42)), the ^{15}N-R_2 relaxation and DEST experiments were acquired after 6 days of incubation at 10 °C, and then HSA was added to an aliquot of the concentrated sample (~7.5 days after sample preparation). Directly after HSA addition, DEST and ^{15}N-R_2 relaxation experiments were acquired again. The incubation at 10 °C for 6 days was essential to reach a pseudo-equilibrium state between monomer and protofibrils in the concentrated samples. In addition, a 3 mM HSA stock solution was prepared specifically for the HSQC monitored titration. The HSA concentration was confirmed by measuring the absorbance at 280 nm using an extinction coefficient of 34,445 M^{-1} cm^{-1} (42, 43). The Aβ peptide concentration was determined by UV absorption at 280 nm with an extinction coefficient of 1,490 M^{-1} cm^{-1} (42, 43). Details about NMR, EM, and DLS data acquisition and processing are available in the supplemental text.

Author contributions—M. A. and G. M. designed the research; M. A., R. A., N. J., and B. A. performed the research; M. A., R. A., N. J., B. A., J. O., and G. M. analyzed data; and M. A. and G. M. wrote the paper.

Acknowledgments—We thank J. C. Lee and M. Gloyd (McMaster) for helpful discussions.

References

1. Karran, E., Mercken, M., and De Strooper, B. (2011) The amyloid cascade hypothesis for Alzheimer's disease: an appraisal for the development of therapeutics. *Nat. Rev. Drug Discov.* **10,** 698–712
2. Biere, A. L., Ostaszewski, B., Stimson, E. R., Hyman, B. T., Maggio, J. E., and Selkoe, D. J. (1996) Amyloid β-peptide is transported on lipoproteins and albumin in human plasma. *J. Biol. Chem.* **271,** 32916–32922
3. Bohrmann, B., Tjernberg, L., Kuner, P., Poli, S., Levet-Trafit, B., Näslund, J., Richards, G., Huber, W., Döbeli, H., and Nordstedt, C. (1999) Endogenous proteins controlling amyloid β-peptide polymerization: possible implications for β-amyloid formation in the central nervous system and in peripheral tissues. *J. Biol. Chem.* **274,** 15990–15995
4. Llewellyn, D. J., Langa, K. M., Friedland, R. P., and Lang, I. A. (2010) Serum albumin concentration and cognitive impairment. *Curr. Alzheimer Res.* **7,** 91–96
5. Boada, M., Ortiz, P., Anaya, F., Hernández, I., Muñoz, J., Núñez, L., Olazarán, J., Roca, I., Cuberas, G., Tárraga, L., Buendia, M., Pla, R. P., Ferrer, I., and Páez, A. (2009) Amyloid-targeted therapeutics in Alzheimer's disease: use of human albumin in plasma exchange as a novel approach for Aβ mobilization. *Drug news Perspect.* **22,** 325–339
6. Boada-Rovira, M. (2010) Human albumin grifols 5% in plasmapheresis: a new therapy involving β-amyloid mobilisation in Alzheimer's disease. *Rev. Neurol.* **50,** S9–S18
7. Anaya, F. (2010) Therapeutic plasmapheresis and experience in Alzheimer's disease. *Rev. Neurol.* **50,** S5–S8
8. Boada, M., Ramos-Fernández, E., Guivernau, B., Muñoz, F. J., Costa, M., Ortiz, A. M., Jorquera, J. I., Núñez, L., Torres, M., and Páez, A. (2016) Tratamiento de la enfermedad de Alzheimer mediante terapia combinada de aféresis terapéutica y hemoféresis con albúmina e inmunoglobulina intravenosa: fundamentos y aproximación terapéutica al estudio AMBAR (Alzheimer Management By Albumin Replacement). *Neurología* **31,** 473–481
9. Costa, M., Ortiz, A. M., and Jorquera, J. I. (2012) Therapeutic albumin binding to remove 7amyloid-β. *J. Alzheimers Dis.* **29,** 159–170
10. Milojevic, J., Esposito, V., Das, R., and Melacini, G. (2007) Understanding the molecular basis for the inhibition of the Alzheimer's Aβ-peptide oligomerization by human serum albumin using saturation transfer difference and off-resonance relaxation NMR spectroscopy. *J. Am. Chem. Soc.* **129,** 4282–4290
11. Milojevic, J., and Melacini, G. (2011) Stoichiometry and affinity of the human serum albumin-Alzheimer's Aβ peptide interactions. *Biophys. J.* **100,** 183–192
12. Milojevic, J. (2012) *Understanding the Inhibition of the Alzheimer's Aβ peptide by Human Serum Albumin*, Ph.D. thesis, McMaster University
13. Milojevic, J., Raditsis, A., and Melacini, G. (2009) Human serum albumin inhibits Aβ fibrillization through a "monomer-competitor" mechanism. *Biophys. J.* **97,** 2585–2594

14. Frydman-Marom, A., Convertino, M., Pellarin, R., Lampel, A., Shaltiel-Karyo, R., Segal, D., Caflisch, A., Shalev, D. E., and Gazit, E. (2011) Structural basis for inhibiting β-amyloid oligomerization by a non-coded β-breaker-substituted endomorphin analogue. *ACS Chem. Biol.* **6,** 1265–1276
15. Scherzer-Attali, R., Pellarin, R., Convertino, M., Frydman-Marom, A., Egoz-Matia, N., Peled, S., Levy-Sakin, M., Shalev, D. E., Caflisch, A., Gazit, E., and Segal, D. (2010) Complete phenotypic recovery of an Alzheimer's disease model by a quinone-tryptophan hybrid aggregation inhibitor. *PLoS One* **5,** e11101
16. Cohen, T., Frydman-Marom, A., Rechter, M., and Gazit, E. (2006) Inhibition of amyloid fibril formation and cytotoxicity by hydroxyindole derivatives. *Biochemistry* **45,** 4727–4735
17. Algamal, M., Milojevic, J., Jafari, N., Zhang, W., and Melacini, G. (2013) Mapping the interactions between the Alzheimer's Aβ-peptide and human serum albumin beyond domain resolution. *Biophys. J.* **105,** 1700–1709
18. Wang, C., Cheng, F., Xu, L., and Jia, L. (2016) HSA targets multiple Aβ42 species and inhibits the seeding-mediated aggregation and cytotoxicity of Aβ42 aggregates. *RSC Adv.* **6,** 71165–71175
19. Ezra, A., Rabinovich-Nikitin, I., Rabinovich-Toidman, P., and Solomon, B. (2016) Multifunctional effect of human serum albumin reduces Alzheimer's disease related pathologies in the 3xTg mouse model. *J. Alzheimers Dis.* **50,** 175–188
20. Raditsis, A. V., Milojevic, J., and Melacini, G. (2013) Aβ association inhibition by transferrin. *Biophys. J.* **105,** 473–480
21. Suzuki, Y., Brender, J. R., Soper, M. T., Krishnamoorthy, J., Zhou, Y., Ruotolo, B. T., Kotov, N. A., Ramamoorthy, A., and Marsh, E. N. (2013) Resolution of oligomeric species during the aggregation of $A\beta_{1-40}$ Using ^{19}F NMR. *Biochemistry* **52,** 1903–1912
22. DeToma, A. S., Salamekh, S., Ramamoorthy, A., and Lim, M. H. (2012) Misfolded proteins in Alzheimer's disease and type II diabetes. *Chem. Soc. Rev.* **41,** 608–621
23. Kotler, S. A., Brender, J. R., Vivekanandan, S., Suzuki, Y., Yamamoto, K., Monette, M., Krishnamoorthy, J., Walsh, P., Cauble, M., Holl, M. M., Marsh, E. N., and Ramamoorthy, A. (2015) High-resolution NMR characterization of low abundance oligomers of amyloid-β without purification. *Sci. Rep.* **5,** 11811
24. Kotler, S. A., Walsh, P., Brender, J. R., and Ramamoorthy, A. (2014) Differences between amyloid-β aggregation in solution and on the membrane: insights into elucidation of the mechanistic details of Alzheimer's disease. *Chem. Soc. Rev.* **43,** 6692–6700
25. Milojevic, J., Costa, M., Ortiz, A. M., Jorquera, J. I., and Melacini, G. (2014) *In vitro* amyloid-β binding and inhibition of amyloid-β self-association by therapeutic albumin. *J. Alzheimers Dis.* **38,** 753–765
26. Fawzi, N. L., Ying, J., Ghirlando, R., Torchia, D. A., and Clore, G. M. (2011) Atomic-resolution dynamics on the surface of amyloid-β protofibrils probed by solution NMR. *Nature* **480,** 268–272
27. Fusco, G., Pape, T., Stephens, A. D., Mahou, P., Costa, A. R., Kaminski, C. F., Kaminski Schierle, G. S., Vendruscolo, M., Veglia, G., Dobson, C. M., and De Simone, A. (2016) Structural basis of synaptic vesicle assembly promoted by α-synuclein. *Nat. Commun.* **7,** 12563
28. Naldi, M., Fiori, J., Pistolozzi, M., Drake, A. F., Bertucci, C., Wu, R., Mlynarczyk, K., Filipek, S., De Simone, A., and Andrisano, V. (2012) Amyloid β-peptide 25–35 self-assembly and its inhibition: A model undecapeptide system to gain atomistic and secondary structure details of the Alzheimers disease process and treatment. *ACS Chem. Neurosci.* **3,** 952–962
29. Bouvignies, G., and Kay, L. E. (2012) Measurement of proton chemical shifts in invisible states of slowly exchanging protein systems by chemical exchange saturation transfer. *J. Phys. Chem. B.* **116,** 14311–14317
30. Vallurupalli, P., Bouvignies, G., and Kay, L. E. (2012) Studying "invisible" excited protein states in slow exchange with a major state conformation. *J. Am. Chem. Soc.* **134,** 8148–8161
31. Long, D., Marshall, C. B., Bouvignies, G., Mazhab-Jafari, M. T., Smith, M. J., Ikura, M., and Kay, L. E. (2013) A comparative CEST NMR study of slow conformational dynamics of small GTPases complexed with GTP and GTP analogues. *Angew. Chem. Int. Ed. Engl.* **52,** 10771–10774
32. Fawzi, N. L., Ying, J., Torchia, D. A., and Clore, G. M. (2012) Probing exchange kinetics and atomic resolution dynamics in high-molecular-weight complexes using dark-state exchange saturation transfer NMR spectroscopy. *Nat. Protoc.* **7,** 1523–1533
33. Ahmed, M., Davis, J., Aucoin, D., Sato, T., Ahuja, S., Aimoto, S., Elliott, J. I., Van Nostrand, W. E., and Smith, S. O. (2010) Structural conversion of neurotoxic amyloid-β(1–42) oligomers to fibrils. *Nat. Struct. Mol. Biol.* **17,** 561–567
34. Yang, M., and Teplow, D. B. (2008) Amyloid β-protein monomer folding: free-energy surfaces reveal alloform-specific differences. *J. Mol. Biol.* **384,** 450–464
35. Xiao, Y., Ma, B., McElheny, D., Parthasarathy, S., Long, F., Hoshi, M., Nussinov, R., and Ishii, Y. (2015) Aβ(1–42) fibril structure illuminates self-recognition and replication of amyloid in Alzheimer's disease. *Nat. Struct. Mol. Biol.* **22,** 499–505
36. Jang, H., Arce, F. T., Ramachandran, S., Kagan, B. L., Lal, R., and Nussinov, R. (2013) Familial Alzheimer's disease Osaka mutant (ΔE22) β-barrels suggest an explanation for the different Aβ(1–40/42) preferred conformational states observed by experiment. *J. Phys. Chem. B* **117,** 11518–11529
37. Miller, Y., Ma, B., and Nussinov, R. (2009) Polymorphism of Alzheimer's Aβ17–42 (p3) oligomers: the importance of the turn location and its conformation. *Biophys. J.* **97,** 1168–1177
38. Jang, H., Arce, F. T., Ramachandran, S., Kagan, B. L., Lal, R., and Nussinov, R. (2014) Disordered amyloidogenic peptides may insert into the membrane and assemble into common cyclic structural motifs. *Chem. Soc. Rev.* **43,** 6750–6764
39. Fawzi, N. L., Ying, J., Torchia, D. A., and Clore, G. M. (2010) Kinetics of amyloid β monomer-to-oligomer exchange by NMR relaxation. *J. Am. Chem. Soc.* **132,** 9948–9951
40. Pace, C. N., Vajdos, F., Fee, L., Grimsley, G., and Gray, T. (1995) How to measure and predict the molar absorption coefficient of a protein. *Protein Sci.* **4,** 2411–2423
41. Paravastu, A. K., Leapman, R. D., Yau, W.-M., and Tycko, R. (2008) Molecular structural basis for polymorphism in Alzheimer's β-amyloid fibrils. *Proc. Natl. Acad. Sci.* **105,** 18349–18354
42. Roche, J., Ying, J., and Bax, A. (2016) Accurate measurement of $^{3}J_{HNH\alpha}$ couplings in small or disordered proteins from WATERGATE-optimized TROSY spectra. *J. Biomol. NMR* **64,** 1–7
43. Roche, J., Shen, Y., Lee, J. H., Ying, J., and Bax, A. (2016) Monomeric Aβ1–40 and Aβ1–42 peptides in solution adopt very similar Ramachandran map distributions that closely resemble random coil. *Biochemistry* **55,** 762–775
44. Manzoni, C., Colombo, L., Bigini, P., Diana, V., Cagnotto, A., Messa, M., Lupi, M., Bonetto, V., Pignataro, M., Airoldi, C., Sironi, E., Williams, A., and Salmona, M. (2011) The molecular assembly of amyloid Aβ controls its neurotoxicity and binding to cellular proteins. *PLoS One* **6,** e24909
45. Teplow, D. B. (1998) Structural and kinetic features of amyloid P-protein fibrillogenesis. *Amyloid* **5,** 121–142
46. Rózga, M., Kłoniecki, M., Jabłonowska, A., Dadlez, M., and Bal, W. (2007) The binding constant for amyloid Aβ40 peptide interaction with human serum albumin. *Biochem. Biophys. Res. Commun.* **364,** 714–718
47. Stanyon, H. F., and Viles, J. H. (2012) Human serum albumin can regulate amyloid-β peptide fiber growth in the brain interstitium: implications for Alzheimer disease. *J. Biol. Chem.* **287,** 28163–28168
48. Kuo, Y. M., Emmerling, M. R., Lampert, H. C., Hempelman, S. R., Kokjohn, T. A., Woods, A. S., Cotter, R. J., and Roher, A. E. (1999) High levels of circulating Aβ42 are sequestered by plasma proteins in Alzheimer's disease. *Biochem. Biophys. Res. Commun.* **257,** 787–791